Combustion, flow and spray dynamics for aerospace propulsion

Study of a liquid–gas mixing layer: Shear instability and size of produced drops

Étude d'une couche de mélange liquide gaz : Instabilité de cisaillement et taille de gouttes produites

Sylvain Marty *, Jean-Philippe Matas, Alain Cartellier

Laboratoire des écoulements géophysiques et industriels (LEGI), CNRS – Université de Grenoble, BP53 38041, Grenoble cedex 9, France

A B S T R A C T

We study experimentally the atomization of a thick liquid film by a parallel gas flow, in order to understand the conditions of destabilization of the liquid film and the conditions of drop creation. We study in particular the regimes at low M (ratio of gas/liquid dynamic pressures), to test the scaling law proposed and validated in previous studies at large M ($M = 16$).

The spatial inviscid stability analysis of the system is carried out with a new velocity profile taking into account the wake of the splitter plate (zero speed at the level of the splitter plate): the influence of liquid velocity on the shear instability frequency turns out to be significantly stronger for this type of velocity profile than for continuous profile.

An asymptotic study of the dispersion relation leads to a new scaling law giving the wavenumber of the shear instability as a function of gas velocity U_g, with a corrective term in M. Frequency measurements carried out by a spectral method show a good agreement with this corrected law.

We investigate by way of optical probe measurements the size distribution of produced drops downstream. The difficulty of these measurements live in the decrease of the number density flux of drops at low M. Results obtained for the mean chord are consistent with previous studies. Diameter distributions are obtained from chord distributions with a numerical conversion procedure.

© 2012 Académie des sciences. Published by Elsevier Masson SAS. All rights reserved.

R É S U M É

Nous étudions expérimentalement l'atomisation d'une nappe liquide par un courant parallèle gaz, afin de comprendre les conditions de déstabilisation de la nappe liquide et les conditions de formation de gouttes. Nous étudions en particulier les régimes de faible M (rapport de pression dynamique gaz/liquide), afin de tester les lois d'échelle mises en évidence lors d'études précédentes et validées sur un régime à grand M ($M = 16$).

L'analyse de stabilité inviscide du système est menée avec un nouveau profil de vitesse prenant en compte le sillage de la plaque séparatrice (vitesse nulle au niveau de la plaque de séparation) : l'influence de la vitesse de phase liquide sur la fréquence de l'instabilité de cisaillement est significativement plus forte pour ce type de profil de vitesse que pour les profils classiques. Une étude asymptotique de la relation de dispersion permet de trouver une nouvelle loi d'échelle reliant le nombre d'onde du mode le plus instable à la vitesse gaz

* Corresponding author.
  E-mail address: Sylvain.Marty@legi.grenoble-inp.fr (S. Marty).

U_g, avec un correctif en M. Les mesures de fréquence réalisées par une méthode spectrale montrent un bon accord avec cette loi d'échelle corrigée.

Connaissant les mécanismes en amont nous nous intéressons également aux distributions de taille de gouttes en aval, mesurées par sonde optique. La diminution du flux numérique de goutte et le changement des plages de vitesse des fluides à faible M rendent les mesures plus complexes. Les résultats sur les cordes moyennes mesurées sont cohérents avec les études précédentes.

1. Assisted atomization for low dynamic pressure ratio

Modern turbojet or cryogenic engines use two-phase nozzles to feed their combustion chamber with fuel and comburant. This kind of injection turns a liquid flow into a spray under the action of a fast gas stream. A good quality of this mixture is needed to optimize combustion. Several geometries exist for these injectors (gaz or fluid centered, with or without recess length, etc.) with various diameters and lengths. A good review of the different techniques for atomization can be found in Lightfoot (2009) [1].

Our experimental set-up models an injector with an infinite liquid jet diameter and a thick liquid film flowing over a prefilming zone (Fig. 1). With this geometry we avoid some instability, like the flapping instability of a round liquid jet. Our injector is composed of two parallel horizontal channels: the bottom channel is fed with water from a overflowing tank. Liquid velocity is in the range from 0.1 to 1 m s^{-1}. The upper channel receives a gas stream from a compressor. The maximum gas velocity is near 100 m s^{-1}. In order to limit velocity perturbations, honey combs are inserted in each channel, a porous plate in the gas one, and each channel ends with a smooth convergent profile (Fig. 1). In addition to the geometrical characteristics of the nozzle and fluid properties we have two main parameters controlling the injection: gas velocity U_g and liquid velocity U_l. The dynamic pressure ratio M can be used in place of either velocity. Previous studies carried out on this set-up have highlighted successive mechanisms of destabilization [4–6]. First a shear instability controlled by the gas vorticity thickness has been clearly identified: this Kelvin–Helmholtz type instability induces longitudinal waves. On the crest of these waves a transverse instability takes place, similar to a Rayleigh–Taylor instability due to the aerial acceleration of the waves (Hong (2003) [6]). The transversal perturbations then turn into ligaments by elongation, and eventually break into droplets (see Raynal et al. (1997) [4] and Marmottant and Villermaux (2004) [5]). One of the most notable result evidenced by these authors is the dependency of the wavenumber k of the most amplified mode of the axial instability on the gas flow vorticity thickness δ_g:

$$k = 1.5 \sqrt{\frac{\rho_l}{\rho_g}} \frac{1}{\delta_g} \tag{1}$$

Wave velocity can be estimated from Dimotakis velocity U_c, deduced from stress continuity [7]:

$$U_c = \frac{\sqrt{\rho_l} U_l + \sqrt{\rho_g} U_g}{\sqrt{\rho_l} + \sqrt{\rho_g}} \tag{2}$$
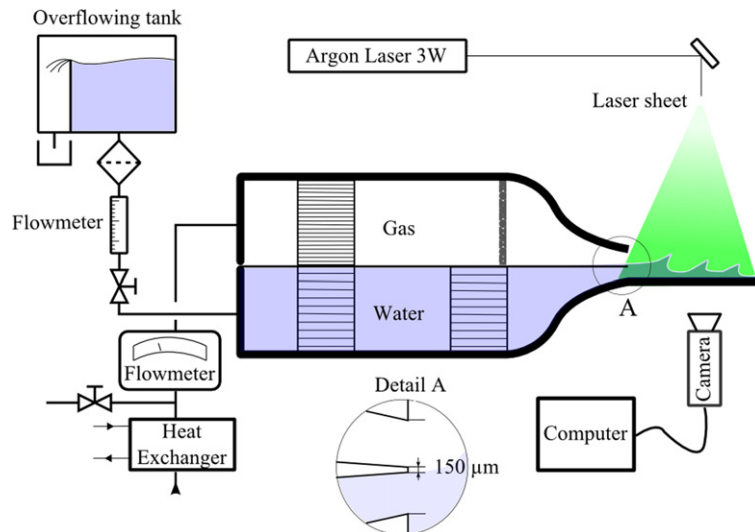

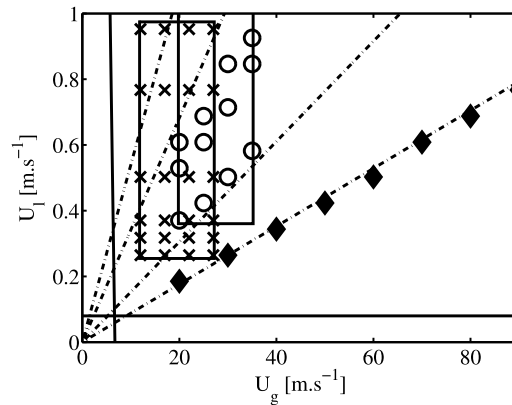**Fig. 1.** Sketch of the experimental set-up.

Fig. 2. Map of experimental points: (◆) $M16$, (×) frequency measurements, (○) droplet size distributions measurements, (-·-·) fixed M value.
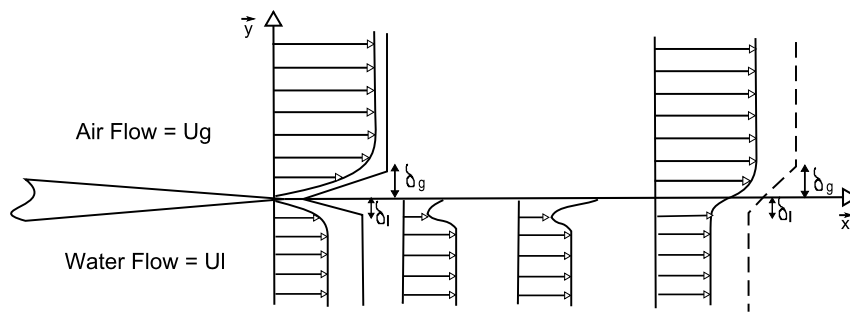

Fig. 3. Donwstream evolution of the velocity profile.

Frequency of the most unstable mode can then finally be approximated as $\omega = kU_c$. Hong (2003) [6] and Ben Rayana (2007) [8] using the same set-up used by Raynal et al. (1997) have focused on a constant $M = 16$ ratio (black diamond series of Fig. 2). These conditions are relevant to cryotechnic engines who use constant injection regime during all the launching time. The case of turboengine for plane is different, from the take off to the cruise at high altitude this injection regime varies from $M = 15$ to 1. In the present study, we vary M to investigate the influence of this parameter on the instabilities. The crosses on Fig. 2 correspond to the frequency measurements of the present study. We will compare the predicted frequency with the measured one. The circle series correspond to the experimental conditions for which droplet size distributions were obtained. A minimum flux of drops is needed in order to ensure a good resolution of the chord pdf: this is why size distributions could not be measured for the same conditions for which frequencies were measured. Finally chord distributions are obtained, these distributions will be presented in Section 5.

2. Asymptotic analysis: influence of a velocity deficit

One of the difficulty in the stability analysis is the choice of a relevant velocity profile for both flows. Rayleigh (1879) [2] and later Chandrasekhar (1981) [3] studied this instability with a finite vorticity thickness in the gas and liquid flow. For their studies Raynal et al. (1997) [4], Marmottant and Villermaux (2004) [5] used this profile to model the final profile far downstream the injection (see Fig. 3), but neglected the vorticity thickness δ_l in the liquid flow [4]. They also showed that in the case of an invicid analysis, the smooth velocity profile (solid line of Fig. 3) can be modeled by a linear one (dashed line of Fig. 3) with $\delta_g = \Delta U_{\max}/\frac{dU}{dy}|_{\max}$.

A new approach, by Matas et al. (2011) [9], takes into account the wake due to the splitter plate: there is a velocity deficit right after the splitter plate. The stability analysis is therefore carried out with the continuous profile represented at the end of the splitter plate. Dispersion relation is solved for a spacial solution. Left Fig. 4 presents the dimensionless frequency obtained with both profiles (dashed line without a deficit, and solid line with a deficit), as a function of M. The gap between the two profiles becomes larger for low M: the frequency is strongly underestimated by the classical analysis for low M. The same effect is observed for the dimensionless growth rate, see right Fig. 4. In order to generalize the prediction of Eq. (1) when the velocity deficit is included, an asymptotic analysis is carried out on the dispersion relation around the unstable mode. Eq. (3) where Ω' and K' are respectively the dimensionless frequency and wavenumber proportional to $\sqrt{\rho_g/\rho_l}$, is this simplified dispersion relation. For obtain this result, it is assumed that M is of order 1 or larger, $\rho_g/\rho_l \ll 1$, $U_l \ll U_g$
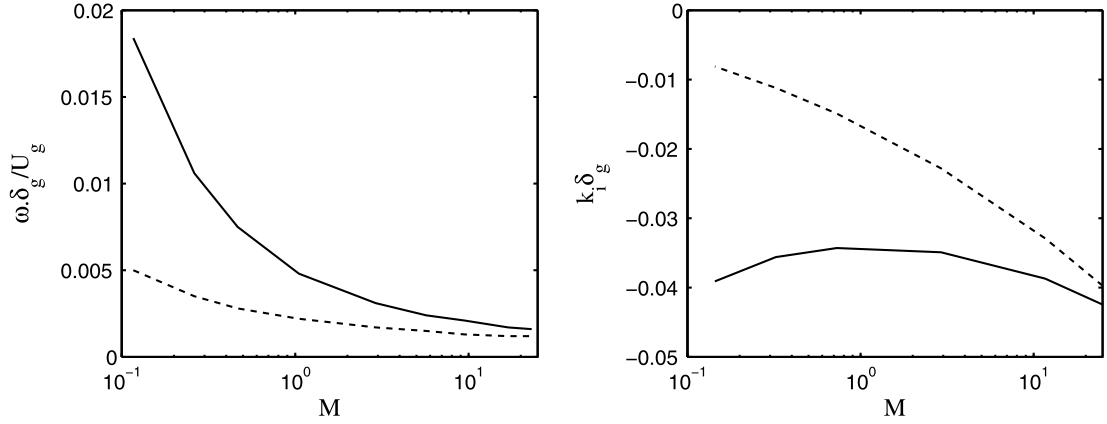
Fig. 4. Dimensionless frequency (left) and growthrate (right) as a function of M obtained with both profiles (dashed line without a velocity deficit, and solid line with a velocity deficit).
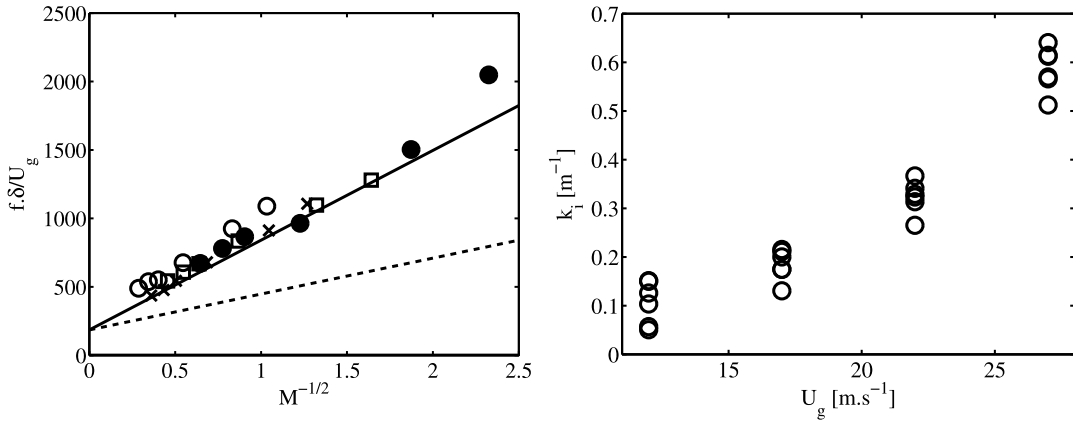

Fig. 5. Shear instability dimensionless frequency (left) and growthrate (right) comparison of experiments with the asymptotic laws derived from the analysis.

and $k\delta_l \ll 1$. The liquid vorticity thickness has to be small compared with the wavelength of the instability.

$$\Omega'^2 - \left(\frac{2K'}{\sqrt{M}} + K'^2\right)\Omega' + \left(\frac{2K'^3}{\sqrt{M}} + K'^2\right) = 0 \qquad (3)$$

This equation is solve for temporal solution. The resulting wavenumber and frequency are:

$$k = \left(\sqrt{2} + \frac{3}{2}M^{-1/2}\right)\sqrt{\frac{\rho_g}{\rho_l}}\frac{1}{\delta_g} \quad \text{and} \quad \omega_r = \frac{\rho_g}{\rho_l}\frac{U_g}{\delta_g}\left(1 + \frac{5}{2}\sqrt{2}M^{-1/2}\right) \qquad (4)$$

This results introduce a corrective term in M to the prediction of Raynal et al. (1997) [4], Marmottant and Villermaux (2004) [5]. In order to test both predictions, frequency was measured for M smaller than 10, i.e. when the corrective term is not negligible.

3. Frequency and growthrate measurements

In order to determine the frequency of the most amplified Kelvin–Helmholtz mode, we use a LIF method. Fluorescein is mixed in the liquid phase, a longitudinal section of the flow is made with an Argon laser, and a high speed camera (Phantom V2) records flow motion in this section. Post treatment of the movie uses a Sobel filter to localize the water surface. We therefore obtain the position h of surface as a function of time and downstream position: $h = f(x, t)$. A Fourier transform of h (Welch method) yields the desired frequency, see Fig. 5. The dimensionless frequency is plotted as a function of $M^{-1/2}$. Experimental series $\bigcirc$, $\square$, $\times$ and $\bullet$ display each gas velocity used, respectively 12, 17, 22 and 27 m/s. Dotted line corresponds to the prediction without a deficit, and solid line to the prediction of Eq. (4).

Experimental points are collapsed around the solid line for all M between 0.25 and 12, in agreement with the analysis where the deficit is included. From the interface position $h = f(x, t)$ we can also draw the variations of wave amplitude downstream the injector. A basic processing has to be carried out, see Ref. [9], in particular to exclude rare events, after
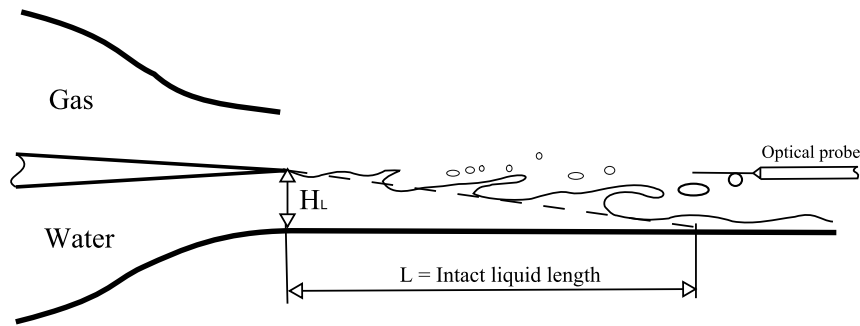
Fig. 6. Relative position of the probe to the spray.

which the spatial growthrate k_i of the longitudinal instability can be obtained. Fig. 5 shows also k_i as a function of gas velocity. The growthrate is mainly a function of gas velocity, but not of M: this behavior is not predicted by the inviscid stability analysis. We believe it results from the large amplitude of the waves, which will itself impacts gas flow, a non-linear mechanism not included in the stability analysis.

4. Droplet size and flux measurements

The previous section has evidenced a significant sensitivity of the axial instability characteristics to the M parameter. The question to be considered now is whether this parameter also alter the size or the flux of the drops produced at the last step of atomization process. We have therefore gathered information of the drops for flow conditions close to those for which frequency and growthrate have been investigated. Droplet size and fluxes have been measured with a monofiber optical probe: detailed information about this sensor and the associated signal processing and post-processing can be found in Ref. [10] and [11]. For the present study, we used an optical probe with a 30 µm sensitive length so that unbiased detection is expected for drops above 10–12 µm. This latency length is measured on a special calibration bench with an uncertainty of about 5 µm. In comparison with previous studies (Cartellier and Ben Rayana (2004) [10] and Hong et al. (2004) [11]) this length is very short and generate some problem of long time scale evolution not clarified now. Independently of these consideration we have a maximum gap between two measurements – of 25% for the mean chord and 31% for the volumetric flux. This repetition of measurement include all the acquisition chain from the selection of injection parameter with the set on of probe to the postprocessing. Note that we cannot exactly cover the same range of conditions as those considered in the previous section. Indeed, for gas velocities below about 20 m s^{-1}, the flux of drops remains very weak and the convergence of the statistics would imply very long acquisition times. In addition, at low gas velocity, the probe dewetting time becomes quite long and may alter the signal quality. This problem is solved by adapting signal processing parameters for each conditions, and by carefully verifying the consistency of each signal.

Hong (2003) [6], who carried out optical probe measurement in a similar configuration, has shown that spatial variations of the measured flux are quite strong, care was also taken, when varying M, to collect data at the same relative position (Fig. 6). When varying M, along the vertical axis the probe is aligned with the splitter plate, and its downstream position is located at the end of the theoretical liquid intact length L. The latter has been shown (Raynal et al. (1997) [4]) to vary as: $\frac{L}{2H_1} \approx \frac{6}{\sqrt{M}}$ here H_1 is the initial water thickness. The first step is to ascertain the convergence of the measurements. We investigated that convergence on the mean chord C_{10} witch is a quantity directly yielded by the optical probe. A typical evolution of the mean chord with number of drops considered is plotted on Fig. 7. As shown by this figure, the mean chord value converges but still exhibits some fluctuation even when the number of drops becomes large. For different gas velocities, we quantified the minimum number of drops that yields a maximum uncertainty of 3% (dashed line) on C_{10} measurements. For $U_g = 20$ m s^{-1}, a minimum of 3000 drops is needed to ensure correspond a convergence of the C_{10} within 3%. For a gas velocity of $U_g = 90$ m s^{-1}, 40 000 drops correspond to a 1.5% uncertainty of the mean chord.

Table 1 provides the mean chords detected for gas velocities evolving between 20 and 35 m s^{-1} and for three values of M, namely 1.5, 2 and 4. It happens that for a given gas velocity, a variation in the M changes the mean chord by a amount varying between 20% and 60%. The lowest M of each U_g always lead the largest drops.

To discuss more precisely this influence, we first introduce the mean chord C_{10} (98%) obtained by removing 2% of the largest chords. The interest of such a filtering is because a few large drops are detected, and it is important to evaluate their relative contribution of the mean. Such as 2% cut-off level was also used by Hong (2003) [6] for the analysis of the data collected at $M = 16$. According to the data in Table 1, the maximum difference between the true mean chord C_{10} and the filtered mean C_{10} (98%) is about 15%.

In addition, that difference is larger at high U_g. Indeed, as U_g increases drops are smaller, so the suppression of even a small amount of large drops has an important impact on the mean. This brings to light the influence of big drops and isolated events on the mean C_{10} value. To investigate this influence, variation of C_{10} as a function of U_g is plotted with different cut-off values for the $M = 4$ set on Fig. 8.
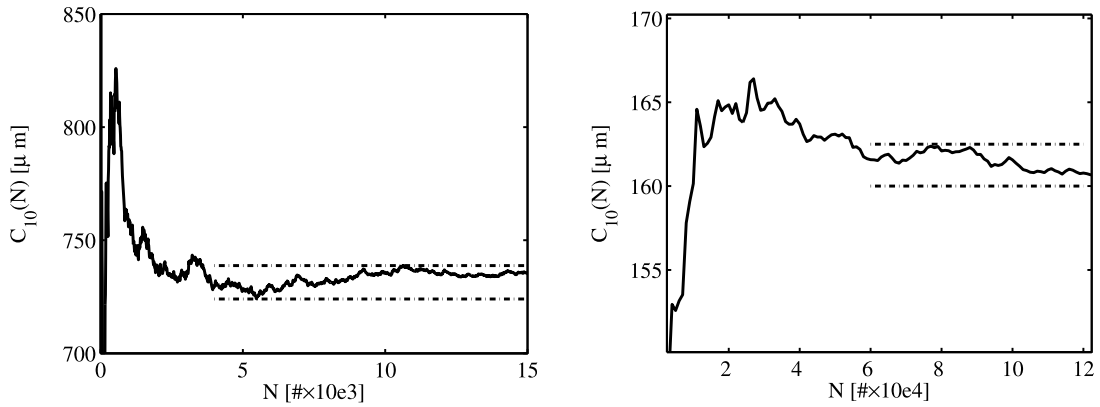
Fig. 7. Convergence of mean chord for (left) $U_g = 30$ m s^{-1} and (right) $U_g = 90$ m s^{-1} at $M = 16$.

Table 1
Mean value of chord length C_{10} [µm] for $M = 4$, $M = 2$, $M = 1, 5$.

U_g	20	20	20	25	25	25	30	30	30	35	35	35
U_l	0.37	0.52	0.61	0.42	0.61	0.69	0.50	0.71	0.85	0.58	0.85	0.93
M	3.4	1.66	1.25	4.06	1.96	1.53	4.15	2.05	1.46	4.21	1.99	1.57
C_{10}	521.8	736.9	853.6	305.1	351.6	375.4	235.3	300.0	327.0	163.2	228.5	265.0
C_{10} (98%)	472.2	663.5	759.4	267.7	310.8	332.2	205.2	259.0	281.3	139.6	192.3	222.6
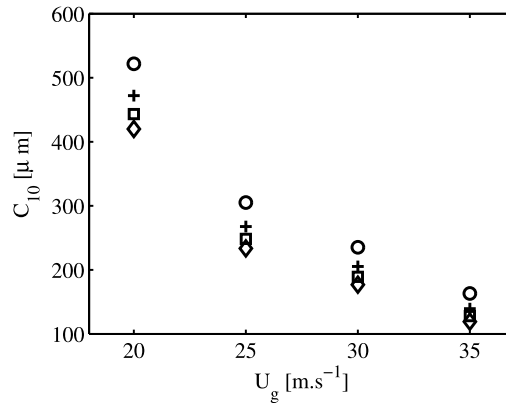
Fig. 8. Variations of C_{10} as a function of U_g for different cut-off values for $M = 4$ set: ($\bigcirc$) 0%; ($+$) 2%; ($\square$) 4%; ($\diamondsuit$) 6%.

As expected the first 2% of eliminated chords ($+$ series) have more influence on the C_{10} than the following cut-offs. This is particularly true for the low U_g. This result clearly indicates that the mean chord is affected by a few rare events, and that removing this stabilizes the drop size.

Now, we can further test the available scaling for the mean drop size. That scaling was based on the following arguments. First, the experiments of Marmottant and Villermaux (2004) [5] demonstrated that the mean droplet diameter is proportional to the transverse instability wavelength. Second, that transverse wavelength was estimated by Hong et al. (2002) [12], Varga et al. (2003) [13], Ben Rayana et al. (2006) [14] by considering the axial acceleration of the wave crest by the air stream and the ensuing Rayleigh–Taylor instability. Third, it was further assumed that the fraction of the wave crest which is atomized is proportional to the axial wavelength, namely $= \alpha \lambda_{axi}$ where λ_{axi} is given by $C_{axi}\sqrt{\rho_g/\rho_l}\,\delta_g$. This model leads to:

$$\lambda_T = 2\pi \sqrt{\frac{6\alpha_n.C_{axi}}{C_d}} \delta_g \left(\frac{\rho_l}{\rho_g}\right)^{1/4} \left(\frac{\rho_G(U_G - U_C)^2 \delta_g}{\sigma}\right)^{-1/2} \tag{5}$$

$$\lambda_T \approx \delta_g \left(\frac{\rho_l}{\rho_g}\right)^{1/4} We_{\delta}^{-1/2} \tag{6}$$

where the drag coefficient C_d is about 2. This model predicts a non-dimensional drop size D/δ_g evolving as $We^{-1/2}$. Such a trend was confirmed by previous experiments performed at $M = 16$: the diamond series in Fig. 9 are the result of Ben
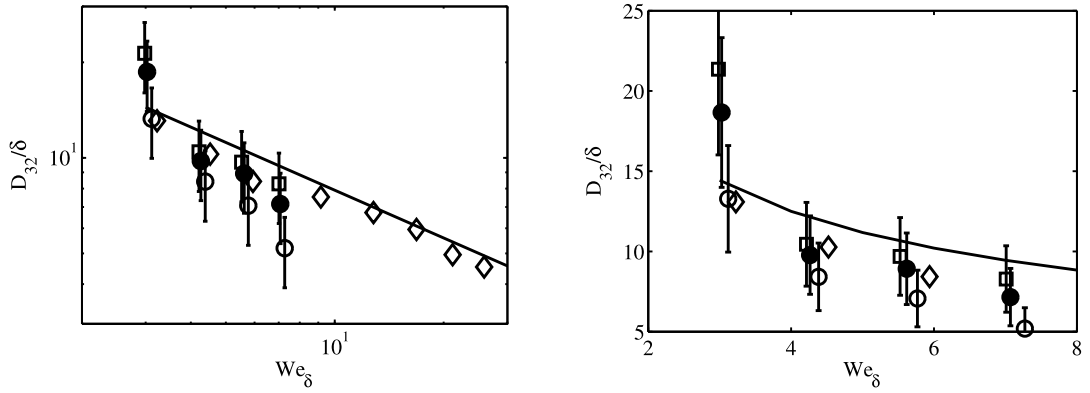
Fig. 9. Dimensionless D_{32} as a function of Weber number (left) and a focus on low M data (right): ($\diamondsuit$) $M16$; ($\bigcirc$) $M4$; ($\bullet$) $M2$; ($\square$) $M1.5$.
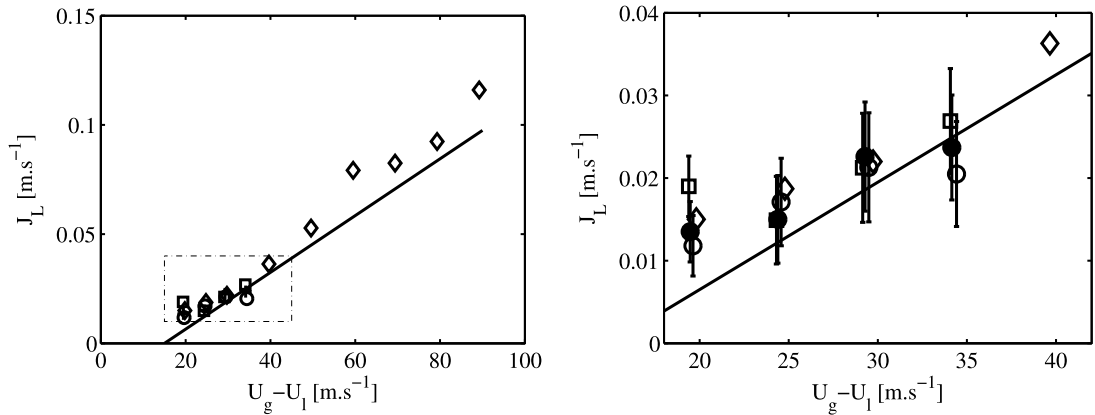

Fig. 10. Volumetric flux J_L as a function of $U_g - U_l$ and a focus on low M data: ($\diamondsuit$) $M16$; ($\bigcirc$) $M4$; ($\bullet$) $M2$; ($\square$) $M1.5$.

Rayana (2007) [8] (collected with another optical probe with a sensitive length about 45 µm). To plot our data collected at low M on this figure, the Sauter mean diameter D_{32} is directly estimated from the C_{10} using $D_{32} = (3/2)C_{10}$ [15]. The drop size measured at low M happen to reasonably agree with predicted trend, except at the lowest gas velocities for witch extra mechanisms alter ligament formation (see Ben Rayana et al. 2006 [14]). Beside the symbols on Fig. 9 are quite close indicating that the prefactor in Eq. (5) is only slightly modified when M is varied. Since the prefactor includes the fraction α of the crest that is stripped off the bulk liquid, this result indicates that the shape of the axial waves remain rather similar for all M. To further confirm the above mentioned trends and more precisely investigate the influence of M, more result at low M and a higher gas velocity are needed: such a campaign will require some adaptation of the existing experiment. Finally, let us consider the volumetric flux J_L of the droplet produced by stripping, this flux corresponds to the entrainment velocity U_e at the interface. The latter can be estimated (Ben Rayana (2007) [8]) by writing down the continuity of turbulent stress at the interface, namely:

$$\rho_L . U_e^2 = C_1 \rho_G u'^2 \tag{7}$$

where u'^2 is the turbulent intensity in the gas phase and C_1 an entrainment coefficient equal to 0.25 in a single phase mixing layer, value done by Hussain and Zedan (1978) [16]. In this case, the velocity fluctuation is estimated to be proportional to the mean velocity difference along: $u' = \alpha'(U_g - U_l)$. The volumetric flux J_L is then given by:

$$J_L = C_1^{1/2} \left(\frac{\rho_g}{\rho_l} \right)^{1/2} \left(\alpha'(U_g - U_l) \right) \tag{8}$$

This simple model predicts J_L to increase as $U_g - U_l$. As shown in Fig. 10 this trend is recovered for all the experimental conditions considered except at the lowest gas velocities. The diamond series (Ben Rayana's data at $M = 16$ [8]) corresponds to the straight line $J_L = (U_g - U_l - 15) \times 0.0013$, where the -15 shift models the absence of atomization below about 15 m s^{-1}. Its slope 0.0013 allows to evaluate an entrainment coefficient C_1 equal to 0.0088 for α' equal to 0.40, value measured from particle image velocity by Descamps et al. (2008) [17]. This small value compared to the value for single
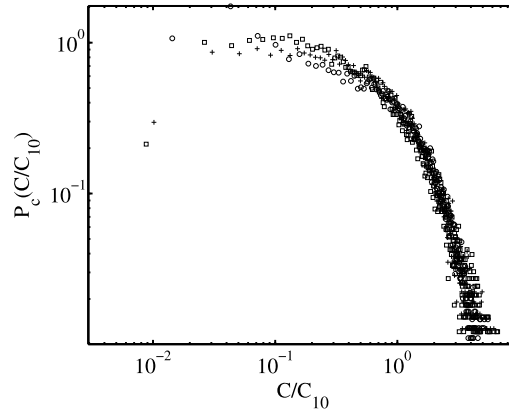
Fig. 11. Dimensionless chord pdf for $U_g = 20$ m s^{-1} at three different M: ($\bigcirc$) $M4$; ($+$) $M2$; ($\square$) $M1.5$.

Table 2
Root mean square of dimensionless chord for $M = 4$, 2 and 1.5.

U_g	20	20	20	25	25	25	30	30	30	35	35	35
$\sigma(C/C_{10})$	1.09	1.09	1.19	1.27	1.24	1.20	1.29	1.39	1.39	1.46	1.53	1.53

phase mixing layer ($C_1 \approx 0.25$) is attributed to the fact that the measure is here localized. In experiments with strong spatial gradients, local data cannot be directly compared with global entrainment rate.

5. Chord pdf

The last step is to check how chord distributions are modified when M is varied for fixed U_g. Fig. 11 is a superposition of the distributions of C/C_{10} for three values of M, for the same U_g: the pdfs are well superposed.

The standard deviation of these pdfs, defined as $\sigma_C = \sqrt{C_{20}/C_{10}^2 - 1}$, are given on Table 2: σ_C increases with U_g, but is roughly constant when M is varied for a fixed U_g. Chord distributions are therefore mainly controlled by U_g.

6. Conclusion

We have carried out frequency and spatial growthrate measurements for the shear instability of a planar two-phase mixing layer. Experimental frequencies were found to agree with the prediction of an inviscid linear stability analysis including a velocity deficit at the interface, while experimental growthrates were much larger than predicted, and exhibited a dependence on U_g not predicted by the analysis. Droplet size measurements were carried out with an optical probe. Drop chord and volumic flux follow the scaling law predicted by known mechanisms, in particular $D_{32}/\delta_g \sim We^{-1/2}$. Prefactor are insensitive to M in the range from 1.5 to 16 for $U_g \leqslant 35$ m s^{-1}. Additional data for larger U_g for the same M are needed to confirm these results.

References

[1] M. Lightfoot, Fundamental classification of atomization processes, At. Sprays 19 (11) (2009) 1065–1104.
[2] Lord Rayleigh, On the stability, or instability, of certain fluid motions, Proc. Lond. Math. Soc. 11 (1879) 57.
[3] S. Chandrasekhar, Hydrodynamic and Hydromagnetic Stability, Dover Publication, 1981, Chapter X.
[4] L. Raynal, E. Villermaux, J. Lasheras, E.J. Hopfinger, Primary instability in liquid gas shear layers, in: 11th Symp. on Turbulent Shear Flows, vol. 3, 1997, pp. 27.1–27.5.
[5] P. Marmottant, E. Villermaux, On spray formation, J. Fluid Mech. 498 (2004) 73.
[6] M. Hong, Atomisation et mélange dans les jets coaxiaux liquide–gaz, Thèse INPG, LEGI, 2003.
[7] P.E. Dimotakis, Two-dimensional shear-layer entrainment, AIAA J. 24 (1986) 1791–1796.
[8] F. Ben Rayana, Contribution à l'étude des instabilités interfaciales liquide–gaz en atomisation assistée et tailles de gouttes, Thèse INPG, LEGI, 2007.
[9] J.P. Matas, S. Marty, A. Cartellier, Experimental and analytical study of a shear instability of a gaz–liquid mixing layer, Phys. Fluids 23 (2011).
[10] A. Cartellier, F. Ben Rayana, Dispersed phase measurements in sprays using optical probes, in: 3rd International Symposium on Two-Phase Flow Modelling and Experimentation, Pisa, 22–24 September 2004.
[11] M. Hong, A. Cartellier, E. Hopfinger, Characterization of phase detection optical probes for the measurement of the dispersed phase parameters in sprays, Int. J. Multiph. Flow (2004).
[12] M. Hong, A. Cartellier, E. Hopfinger, Atomisation and mixing in coaxial injection, in: 4th Int. Conference on Launcher Technologie "Space Launcher Liquid Propulsion", Liège, 3–6 December 2002.
[13] C.M. Varga, J.C. Lasheras, E. Hopfinger, Initial breakup of a small-diameter liquid jet by a high-speed gas stream, J. Fluid Mech. 497 (2003) 405–434.
[14] F. Ben Rayana, A. Cartellier, E. Hopfinger, Assisted atomization of a liquid layer: investigation of the parameters affecting the mean drop size prediction, ICLASS, Kyoto, August 27–September 1, 2006.

[15] W. Liu, N.N. Clark, Relationships between distributions of chord lengths and distributions of bubble sizes including their statistical parameter, Int. J. Multiph. Flow 21 (6) (1995) 1073–1089.

[16] A.K.M.F. Hussain, M.F. Zedan, Effects of the initial condition on the axisymmetric free sheer layer: effects on the initial momentum thickness, Phys. Fluids 21 (7) (1978) 1100–1112.

[17] M. Descamps, J.-P. Matas, A. Cartellier, Gas–liquid atomisation: gas phase characteristics by PIV measurements and spatial evolution of the spray, in: 2nd Colloque INCA, 23–24 October 2008.